ChemElectroChem

Research Article
doi.org/10.1002/celc.202400323

Chemistry Europe
European Chemical Societies Publishing

www.chemelectrochem.org

Composite Separators with Very High Garnet Content for Solid-State Batteries

Kevin Vattappara,[a, c, d] Martin Finsterbusch,[b] Dina Fattakhova-Rohlfing,*[b, c, d] and Andriy Kvasha[a, c]

Lithium-metal solid-state batteries are attractive as next generation of Li-ion batteries due to higher safety and potentially higher energy density. To improve processability, solid-composite separators combine advantages of inorganic and polymer separators in hybrid structure. We report a systematic approach to fabricate composite separators with high content (90–95 wt%) of ceramic Li-ion conducting $Li_{6.45}Al_{0.05}La_3Zr_{1.6}Ta_{0.4}O_{12}$ (LLZO) powder embedded in a polyethylene oxide (PEO)-LiTFSI (20:1) matrix and understand factors affecting their properties and performance. Separators with good mechanical flexibility and excellent thermal stability were obtained, by optimizing materials and processing parameters. It was found that PEO molecular weight strongly influences the microstructure and electrochemical properties of the separators. In optimized separator with 90 wt% of LLZO and PEO with Mw 300,000 g/mol, a total ionic conductivity of 1.4×10^{-5} S/cm at 60 °C was achieved. The ceramic-rich separator showed excellent long-term cycling stability for more than 460 cycles (1000 h) at 0.1 mA/cm^2 in Li/Li symmetrical cells and achieved a critical current density of 0.25 mA/cm^2. The separators also enabled initial discharge capacities of more than 160 mAh/g in full cells with Li metal anode and composite solid-state $LiNi_{0.6}Co_{0.2}Mn_{0.2}O_2$ cathode, although rapid capacity fade was observed after 10 cycles in fully solid-state configuration.

1. Introduction

Lithium-ion batteries (LIBs) are currently the best choice for electric cars, stationary energy storage solutions, consumer electronics etc.[1] Increasing requirements like driving range and fast charging demand higher energy density, good shelf life and safer batteries.[2] The high energy density requirements for batteries can be facilitated with the introduction of high-voltage (HV) cathode materials such as $LiCoO_2$ (LCO),[3] $LiNi_{0.5}Mn_{1.5}O_4$ (LMNO)[4] and LiNixCoyMnzO$_2$ (NMC).[5] Different cycling conditions used currently in LIB's such as fast charging and high-duty operations, highlight the various safety concerns. Some of them can be due to unstable HV behaviour, Li dendrites formation issues owing to lithium deposition during fast charging, thermal runaway and high flammability of liquid electrolytes based on organic solvents.

Solid-state batteries (SSBs) have potential for further developments which could cater to the desired safer operational conditions. The application of solid electrolytes (SE) in SSBs, replacing the highly flammable liquid electrolytes of LIBs, improve battery safety and could be helpful in preventing various hazards. The traditional classifications for solid electrolytes are: (a) solid inorganic electrolytes – SIE and (b) solid polymer electrolytes – SPE. SIE class of electrolytes are known for their thermal and chemical stability among other benefits.[6] SPE class of electrolytes have several advantages such as low-cost synthesis, mechanical flexibility and easy processibility.[7–8] However, each solid electrolyte system individually has some disadvantages impeding their application in commercial SSBs. SPE's based on PEO typically have low ionic conductivity at room temperature and limitations for high-voltage application.[9] On the other hand, most SIEs are generally considered to be brittle, sensitive to humidity, have poor interfacial compatibility and challenging processing (requirements of high-pressure processing and high temperature sintering).[10–11] In this context, solid composite electrolyte (SCE) separators which consist of essentially high-content of Li-ion conductive ceramics mixed with flexible polymers which don't require to be sintered, could be a very attractive solution.

SCE separators are generally engineered to have blend of properties of both electrolyte classes such as processibility of SPE with electrochemical and thermal stability of SIE fillers.[12–15] The classification of SCEs can be based on the chemical nature

[a] K. Vattappara, Dr. A. Kvasha
CIDETEC
Basque Research and Technology Alliance (BRTA)
P. Miramón 196, 20014 Donostia-San Sebastián, Spain

[b] Dr. M. Finsterbusch, Prof. Dr. D. Fattakhova-Rohlfing
Institute of Energy Materials and Devices (IMD-2): Materials Synthesis and Processing
Forschungszentrum Jülich GmbH
Wilhelm-Johnen-Straße, 52428 Jülich, Germany
E-mail: d.fattakhova@fz-juelich.de

[c] K. Vattappara, Prof. Dr. D. Fattakhova-Rohlfing, Dr. A. Kvasha
FR CNRS 3104
Hub de l'Energie
ALISTORE-European Research Institute
15 Rue Baudelocque, Amiens 80039, France

[d] K. Vattappara, Prof. Dr. D. Fattakhova-Rohlfing
Faculty of Engineering and Center for Nanointegration Duisburg-Essen CENIDE
Universität Duisburg-Essen
Lotharstraße 1, 47057 Duisburg, Germany

Supporting information for this article is available on the WWW under https://doi.org/10.1002/celc.202400323

of fillers, the morphology of fillers and the content of fillers present in separator matrix. Depending on the amount of fillers present in separator matrix, SCE's can be classified as low content which is considered to between 1–50 wt%[16] and high content which is higher than 50 wt%.[13,17] Composite separators with high content of ceramics are reported to show characteristic ceramic behaviour such as non-flammability, high thermal and electrochemical stability.[18]

There have been several works carried out on exploring the niche class of ceramic rich composite separator systems, where the ceramic content present in the electrolytes is more than 50 wt%. Choi and collaborators[19] investigated different contents (0, 42.5, 52.5, 62.5, 72.5, and 82.5 wt%) of tetragonal phase LLZO powder in the PEO matrix. They found that the highest ionic conductivity was observed at 52.5 wt% of LLZO in their work. Some other works have pushed the upper limit on content of ceramic fillers added in a polymeric/organic matrix. Guo *et al.*[20] prepared composite electrolytes based on LAGP powder in PEO matrix at a high content up to 99 wt% of LAGP. Different morphologies of fillers have also being investigated in this class of separators, Cai and co-workers[21] prepared a conductive composite electrolyte based on 3D LLZO framework (56 wt%), which exhibited ionic conductivity values of 2.51×10^{-4} S/cm at room temperature and high Li^+ transference number of 0.61. It should also be noted that sometimes due to high content of inorganics in the electrolyte matrix, it may be necessary to provide additional support with external substrates. Kim *et al.*[22] prepared SCE with 70 wt% of Al doped LLZO and PEO-$LiClO_4$, which was cast on polyethylene terephthalate (PET) film as support, which exhibited ionic conductivity values of ~7.6×10^{-6} S/cm at 25 °C and ~1.9×10^{-3} S/cm at 70 °C.

Despite recent interest, ceramic-rich composite electrolyte separator systems need extensive studies on understanding Li-ion conduction mechanisms and other parameters to become viable for practical application in SSBs. Examples of various parameters that require further understanding in these separators include: (a) format, (b) processing methods, (c) choice of ceramic fillers, and (d) organic matrix components. The research carried out in this class of ceramic-rich separators, fixate on using $LiFePO_4$ (LFP) based cathode[13,20,21,23–28] for testing and reporting of electrochemical performance. The real-world application in batteries also demand requirements such as compatibility of separators with high-energy cathode active materials, compatibility with Li metal anode, easy processability and scalability, mechanical flexibility and thermal stability.[22] However, there are some works which have reported electrochemical results with NMC based cathodes.[22,26,29,30]

In this work, we are studying the concept of inorganic ultra rich SCE separators (henceforth mentioned as INURSE separators), which are prepared with very high content of Li-ion conductive LLZO powder in PEO-LiTFSI matrix. Even though by formulation, we are close to that of an inorganic pellet which requires high sintering temperatures and times. We were able to prepare mechanically stable and flexible separators with simple processability and promising electrochemical performance. These separators are model systems prepared with a simple solvent-casting process which attempts to understand and report the influence of very high content of LLZO and different molecular weight of PEO on the structural and electrochemical properties of the separator. The ethylene oxide (EO): lithium (Li) ratio in PEO-LiTFSI was kept constant at EO:Li – 20:1 to form a self-standing and flexible separator membrane. Figure 1 shows all separators prepared in this work with their respective content of LLZO and molecular weight of PEO. The separators prepared with 90 wt% and 95 wt% of LLZO in PEO-LiTFSI matrix were tested and compared to reference composite electrolyte containing 43 wt% of LLZO, which was investigated in an earlier work by Thieu *et al.*[31] This work provides insights

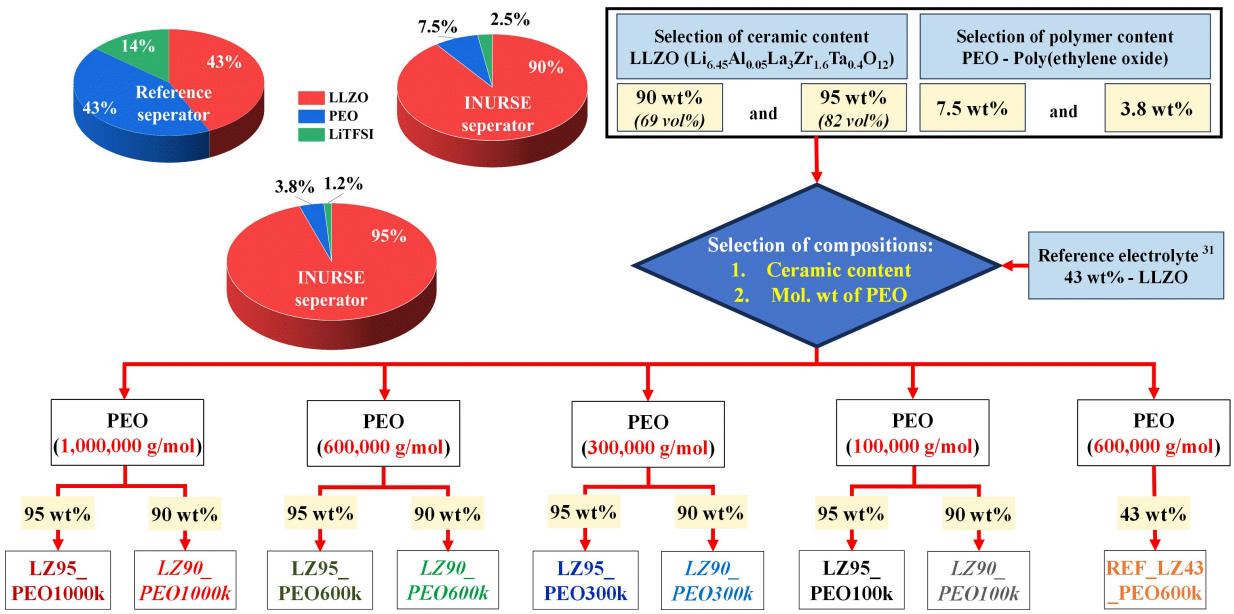

Figure 1. Scheme showing the different components and their composition in the study, carried out to understand the properties of inorganic ultra-rich class of solid electrolyte (INURSE) separators.

on the behaviour of INURSE separators in various electrochemical tests such as for ionic conductivity, galvanostatic cycling of symmetric Li/Li cells etc. INURSE separators exhibited good stability towards Li metal anode during long-term cycling of Li/Li cells. Furthermore, we assessed the HV performance of the INURSE separators in Li metal solid-state coin cells with $LiNi_{0.6}Co_{0.2}Mn_{0.2}O_2$ – NMC622 based solid state composite cathode with a loading of ~1.0 mAh/cm^2.

Experimental

Chemicals

Polyethylene oxide of different molecular weights – 1,000,000 g/mol (PEO1000 K), 600,000 g/mol (PEO600k), 400,000 g/mol (PEO400k), 300,000 g/mol (PEO300k), and 100,000 g/mol (PEO100k); was purchased from Sigma-Aldrich. PEO powders were dried at 55 °C for 16 h under vacuum before usage. Aluminium oxide (Al_2O_3, 99.99%) was purchased from Sigma-Aldrich. Lithium bis(trifluoromethanesulfonyl)imide (LiTFSI, 99.9%) was purchased from Solvionic and used as received. Anhydrous acetonitrile (ACN, 99.8%) used for preparation of both separator and cathode slurry, was purchased from Sigma-Aldrich. Commercial grade single-crystal $LiNi_{0.6}Mn_{0.2}Co_{0.2}O_2$ was purchased from Targray to be used as cathode active material (CAM). 1-Butyl-1-methylpyrrolidiniumbis(trifluoromethanesulfonyl)imide (PYR_{14}TFSI 99.9%) was purchased from Solvionic and used as received. C-ENERGY Super C45 conductive carbon black was purchased from IMERYS Carbon & Graphite, the C45 was stored at 110 °C.

Preparation of INURSE Separators

INURSE separators were prepared in a dry room facility (with a dew point below −45 °C) by a simple and reproducible process, which could be easily upscaled for transfer to industrial processing. A schematic representation of the preparation process is depicted in Figure 2. As the 1st step, LiTFSI and PEO (with different molecular weights), were weighed and added to acetonitrile (ACN) solution. The dissolution was isolated with paraffin film to prevent evaporation of ACN and entry of any aerial contaminants. The PEO-LiTFSI-ACN dissolution was mechanically mixed (EUROSTAR 60 digital, IKA) at 250 rpm overnight to obtain a homogenous PEO-LiTFSI (EO:Li - 20:1) solution. Before adding sieved LLZO powder, speed of the mixer was increased to 1000 rpm. After LLZO powder addition, speed of the dispersion was then increased to 1200 rpm and stirred continuously for 2 h. It needs to be mentioned that, since LLZO is air and humidity sensitive, special care was taken to reduce the exposure as much as possible.

To compare the performance of INURSE separators with an already established composite electrolyte (LLZO and PEO-LiTFSI based) systems, a reference electrolyte separator was also prepared. The formulation and entire preparation procedure can be found in an earlier publication.[31] There were some changes made in the reference separator preparation procedure in this work compared to earlier work. The changes include (i) LLZO: *previous work* – doped with Nb and prepared via ball-milling and SSR route, *current work* – doped with Al and Ta and prepared via modified SSR route and (ii) "solid/solvent" ratio in preparation: *previous work* – 1:9, *current work* – 1:7.

Doctor blade type applicator was used for casting of all prepared slurries onto a 50 μm thick double-side silicone coated film (UK Insulations Ltd) fixed on a substrate. A quadrangular applicator (Nuertek, 60 mm width) was used for slurry casting on the silicone film at an application speed of 50 mm/s. Applicator GAP values of 1500 μm for INURSE and 3000 μm for REF electrolyte separators were selected. The cast separator sheets were first left to dry at room temperature in the dry room and then further dried at 60 °C at reduced pressure of 10 mbar for 40 h to remove traces of ACN solvent. After separators were dried, post processing steps were carried out to prepare for physical-chemical and electrochemical characterizations.

After drying of separators, they were punched with a die into discs with diameter of 18.92 mm. These discs were then hot-pressed (Polystat 200T) at 100 bar (~10 MPa) pressure at 60 °C for 1 minute. The hot-pressing step was done to improve the surface morphology and reduce porosity in the separators. After the hot-pressing step, the ceramic-rich separator discs were punched to the final

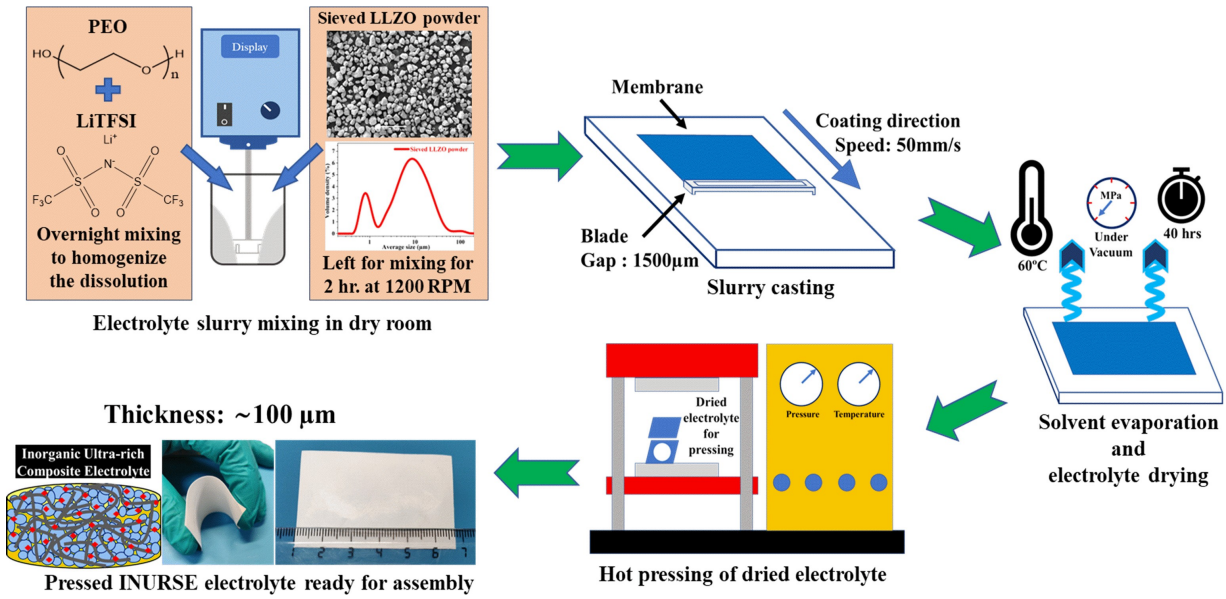

Figure 2. Scheme of preparation process for INURSE separators.

diameter of 18.2 mm. For carrying out electrochemical characterization in coin cells, a detailed coin cell preparation procedure is described in *Supplementary Information*.

Preparation of $LiNi_{0.6}Mn_{0.2}Co_{0.2}O_2$ Based Solid State Composite Cathode

A solid-state composite cathode was created as a model electrode for this work, which was used only for comparative testing purposes for the prepared solid electrolyte separators. The composite cathode was prepared using commercially available materials and a reference formulation. NMC622 based composite cathode was prepared by slurry casting method which could be easily upscaled. The composite cathode slurry was prepared by mechanical mixing using DISPERMAT LC30 dissolver. The formulation for cathode slurry consists of $LiNi_{0.6}Mn_{0.2}Co_{0.2}O_2$ (NMC622) as the active material, SPE "PEO400k/LiTFSI/PYR_{14}TFSI" as catholyte and C-ENERGY Super C45 carbon black as electronic conductor. The composite cathode was prepared with polymer-Li salt-ionic liquid based catholyte to improve Li ion transport, plasticity in microstructure and reduce resistance of "cathode/INURSE separator" interface.

The slurry preparation started with dissolution of "PEO-LiTFSI-PYR_{14}TFSI (25 wt%)" mixture overnight at 250 rpm in ACN solvent. In next step, C45 carbon black (5 wt%) was added to slurry with appropriate amount of ACN to compensate for viscosity increase. In the final step, NMC622 powder (70 wt%) was added slowly to slurry with intermittent addition of ACN to compensate for any change in viscosity. The solid to solvent ratio for cathode preparation was maintained at 1 : 1.7. During the entire preparation process, careful considerations were taken to maintain a constant temperature for the slurry, to prevent change of viscosity. After completion of mixing process, cathode slurry was casted onto 22 μm thick carbon coated aluminium current collector (Gelon). Cathode sheets were dried in air at 55 °C for 3 h. The loading of composite cathode was checked and confirmed to be in range of 8.1–8.7 mg/cm^2, which corresponds to an areal capacity value of 0.99–1.07 mAh/cm^2. After drying, cathodes were calendered at room temperature in a hydraulic calender machine (DPM Solutions) to increase the density up to 2.5 g/cm^3. Calendered cathodes were then punched into discs with high precision cutting dies (El-Cell, Germany) with diameter of 16.6 mm. The cut cathode discs were then dried at 60 °C for 40 h in a vacuum oven (Memmert VO400, $<$10 mbar) in dry room before coin cell assembly.

Physical-chemical Characterization

X-Ray diffraction (XRD) measurements were carried out for synthesized LLZO powder with Bruker D4 Endeavour instrument using Cu–Kα radiation, data was recorded in the 2θ range of 10–80 degrees with a scan rate of 0.02 degree/min. The XRD measurements for the prepared INURSE separators were done with Bruker AXS D8 Advance with Cu Kα radiation, data was recorded in 2θ range of 10–80 degrees with a scan rate of 0.01 degree/min. Cross-sectional and surface morphologies of INURSE separators were analyzed by Scanning Electron Microscope (SEM) – JEOL JSM-5500LV. Sample preparation procedure of post-processed INURSE separators included mounting of separator fragments using carbon tape on Al pin-mounts and Au sputter-coated (60 mA, 50 seconds, 1 mbar). For cross-sectional morphology, additional steps were carried out, post-processed separators were dipped in liquid N_2 for 20 minutes and fragmented to reveal cross-section of separators. Surface and cross-sectional imaging of long-term cycled Li/Li symmetric cell with LZ90_PEO300k was carried out in Zeiss Ultra plus SEM with field-emission source. Cycled cells was disassembled in dry room and samples were transferred to FE-SEM using DME sample transfer shuttle. Particle size distribution (PSD) of LLZO powder (after synthesis and after sieving) was carried out using laser diffraction-based Mastersizer 3000 from Malvern Instruments Ltd. (IESMAT) with Hydro-EV wet-powder dispersion attachment. PSD at different volume distributions was calculated by Mastersizer 3000 software (v3.40) from the acquired light scattering pattern using Mie and Fraunhofer theory. The particle sizes were reported at 10% (Dv10), 50% (Dv50), and 90% (Dv90) of powder volume. The measurements for each powder were carried out in quintuplicate. Thermal properties of separators were assessed using differential scanning calorimetry (DSC, TA Instruments Discovery DSC25 Auto) and thermo-gravimetric analysis (TGA, TA instrument Q500). DSC measurements were recorded at 10 °C/min from −80 °C to 200 °C for a *heat-cool-heat-cool-heat* cycle. To determine glass transition temperature (T_g) of the investigated samples DSC traces were analysed with TRIOS software (V5.6.0.87). TGA measurements were recorded under air atmosphere from 40 °C to 600 °C at a heating rate of 10 °C/min.

Electrochemical Characterization

Ionic conductivity (σ) of the prepared solid separators was measured in symmetric cells with stainless steel (SS) electrodes. Electrochemical Impedance Spectroscopy (EIS) measurements were performed using 1470E potentiostat coupled with 1455 FRA interface (Solartron Analytical). AC sinusoidal signal with an amplitude of 5 mV was applied in a 1 MHz–0.1 Hz frequency range. The symmetrical SS/SS coin cell was initially heated up to 80 °C and held at the temperature for 2 h to completely remove thermal or processing history of the sample. EIS measurements were carried out while cooling from 80 °C to 30 °C at 10 °C interval, with cells stabilized at each temperature for 90 minutes. The ZView software 3.5e (Scribner) was used to fit the obtained impedance spectra to equivalent circuit model (ECM).

The determination of Li^+ transference number for INURSE separators was carried out by Bruce-Vincent-Watanabe method using symmetric Li/Li cells at 60 °C. More details regarding the transference number test can be found in detail in an earlier published work.[31] Symmetric Li/Li cells were also assembled and tested for determining critical current density (CCD) values and studying long-term cycling behaviour for INURSE separators with Li metal anode. For CCD measurements, Li/Li symmetric cells with INURSE separators were cycled with 1 h step at different current density values: 0.01, 0.02, 0.05, 0.1, 0.25, 0.5, 0.75, 1., 1.25, 1.5, 1.75, and 2 mA/cm^2. Long-term cycling of Li/Li symmetric cells were assessed at current density of 0.01 mA/cm^2 and 0.1 mA/cm^2. To understand the practical applicability of INURSE separators, Li/INURSE/Li cells were tested with a protocol combining both critical current density and long-term cycling. The cells started cycling with CCD protocol with 1 h step at current density values of 0.01, 0.02, 0.05, 0.1 until 0.2 mA/cm^2 and maintained at 0.2 mA/cm^2 for long-term cycling until failure. Floating test to assess the electrochemical stability in NMC/Li cell was performed at 60 °C according to the method described in *Supplementary Information*. Galvanostatic charge-discharge cycling was carried out at 0.05 C for charge and 0.1 C for discharge within the cycling range of 3.0–4.2 V and 3.0–4.3 V in Li/NMC622 solid state coin cells. All the electrochemical tests were carried out at 60 °C using BaSyTec cell test system (Germany). Noteworthy, no additional pressure other than coin cell spring was applied during the testing.

2. Results and Discussion

2.1. Preparation and Microstructure Characterization

The process for preparing INURSE separators is shown schematically in Figure 2 and described in detail in *Section 2.2*. In brief, a homogenized slurry containing LLZO powder and PEO-LiTFSI solution was cast as a membrane on a silicone coated support and dried under vacuum at 60 °C to remove ACN solvent. Dried membranes were punched to obtain disks, which were hot pressed at pressure of 100 bar (~10 MPa) at 60 °C for one minute to obtain flexible, mechanically stable separators that were used for further characterization.

Hot pressing of INURSE separators as part of post-processing proved to be essential for improving surface morphology and increasing relative density of the separators. For hot pressing to be effective, melting temperature (T_m) of polymeric matrix was taken into account. DSC measurements showed that all INURSE separators had T_m values below 60 °C. The pressure required for hot pressing was carefully selected after several trials. Another important step was the optimization of size distribution of LLZO powders (Figure S2 b–f), and particularly the reduction of fraction of large agglomerates, which was achieved by sieving the milled powder. The trimodal particle size distribution (PSD) of as-synthesized powder changes after sieving to a bimodal PSD with predominately particles with a size of 7.5 μm and a smaller fraction of particles with a size of about 0.9 μm (Figure S2 b and Table S1 in *Supplementary Information*).

Slurries with ceramic content of 90 wt% and 95 wt% (designated LZ90 and LZ95, respectively) were used to prepare INURSE separators. For each relative ceramic content, PEO with different molecular weight from 10^5 g/mol (designated PEO100k) to 10^6 g/mol (designated PEO1000k) were tested. The prepared INURSE samples, which were named according to LLZO content and molecular weight of PEO polymer, are listed in Table 1 (e.g., sample LZ95_PEO1000k contains 95 wt% sieved LLZO powder and PEO with a molecular weight 10^6 g/mol). The PEO/LiTFSI ratio was set at 20:1 for all samples.

The structural stability of ceramic-rich separators strongly depends on the molecular weight of PEO and is generally improved when PEO with a high molecular weight is used. Thus, for LLZO powders used in this work, no mechanically stable separators could be obtained with PEO with the lowest molecular weight of 10^5 g/mol. In contrast, self-standing and flexible separators with a thickness of 50–150 μm was fabricated with LLZO as ceramic filler and a polymeric matrix consisting of LiTFSI and PEO of higher molecular weights – 3×10^5 g/mol, 6×10^5 g/mol and 10^6 g/mol (shown by means of digital photographs in Figure 3a–c). It should be noted that although fabrication of ceramic-rich separators with low molecular weight polymer binders has already been described by some groups,[32] they have reported the usage of thermal curing/polymerization was required to ensure sufficient mechanical stability, which could complicate the fabrication process.

Scanning electron microscopy (SEM) images of the fabricated INURSE separators in Figure 3d–g, show that they consist of LLZO particles dispersed and pressed together in a polymer matrix with the PSD of sieved LLZO powder. However, the microstructure is strongly influenced by relative ceramic content and PEO molecular weight. INURSE separators prepared with high molecular weight PEO of 10^6 g/mol (LZ90_PEO1000k and LZ95_PEO1000k as seen in Figure S5 a–d) show an inhomogeneous dispersion of LLZO particles in the polymer matrix. In LZ95_PEO1000k separator (in Figure S5 a and S5 b), there are very small number of areas where we observe a dense and connected microstructure of the ceramic particles embedded in the PEO1000k-LiTFSI matrix. In contrast, other areas do not contain enough polymeric matrix, which results in relatively high porosity and poor particle binding. The reason for this behaviour in LZ95_PEO1000k separator, can be attributed to their lower volume fraction and increased viscosity of PEO-LiTFSI solutions due to higher PEO molecular weight.[33] The increased viscosity due to entanglements of the long

Table 1. List of SCE's prepared in this work.

INURSE sample name	LLZO		Molecular weight of PEO (g/mol)	Remarks on the prepared INURSE separators	
	wt%	vol %		Film-formation	Surface topology
LZ95_PEO1000k	95	82	1,000,000	Yes	Rigid surface with pores
LZ90_PEO1000k	90	69	1,000,000	Yes	Rigid surface with pores
LZ95_PEO600k	95	82	600,000	Yes	Smooth surface with higher pore count
LZ90_PEO600k	90	69	600,000	Yes	Smooth surface with less pores
LZ95_PEO300k	95	82	300,000	Yes	Smooth surface with less pores
LZ90_PEO300k	90	69	300,000	Yes	Smooth surface with less pores
LZ95_PEO100k	95	82	100,000	No	No separator formation
LZ90_PEO100k	90	69	100,000	No	No separator formation
REF_LZ43_PEO600k	43	16	600,000	Yes	Soft and smooth due to high content of polymer
REF_$Al_2O_3$90_PEO600k	90	74	600,000	Yes	Rough surface with pores

Note: The separators were prepared with LLZO powder (≤ 25 μm) and PEO-LiTFSI mixture (EO:Li – 20:1).

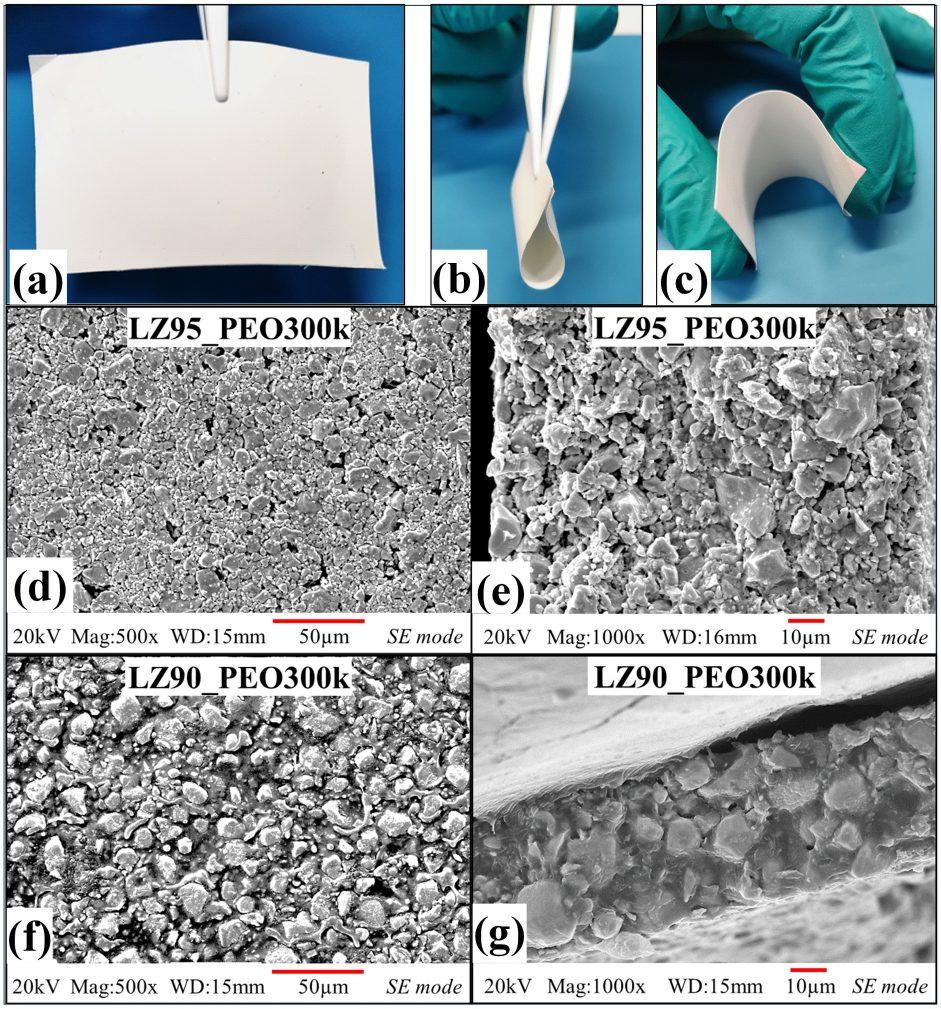

Figure 3. (a–c) Digital photographs showing the self-standing nature and flexibility of LZ95_PEO300k; SEM images of (d–e) LZ95_PEO300k and (f–g) LZ90_PEO300k.

polymer chains[34] leads to reduced flowability of the electrolyte slurry during casting affecting final microstructure.

On the other hand, LZ95_PEO300k separator (in Figure 3d and 3e) prepared with 95 wt% LLZO and PEO300k displayed a denser and more uniform surface and cross-section compared to LZ95_PEO1000k separator. This change in microstructure can be attributed to decrease in molecular weight of the PEO use in the matrix, which after hot-press (during post processing) have higher possibility of compaction. Most optimal microstructure was obtained by INURSE separator with 90 wt% LLZO and PEO with a molecular weight of 3×10^5 g/mol (LZ90_PEO300k) (Figure 3f and 3 g). LZ90_PEO300k shows a dense morphology with a uniform distribution of polymer and LLZO particles. Comparing LZ90_PEO300k to LZ95_PEO300k separator, both the surface and cross-sectional images show a more connected matrix with the LLZO particles with lesser number of pores. SEM images for other compositions can be found in Figure S5 in the *Supplementary Information.*

2.2. Thermal Properties

Figure 4a shows the crystallinity (χ) and glass transition temperature (T_g) for all INURSE and reference separators prepared in this work. All separators with 95 wt% LLZO show lower T_g values compared to 90 wt% LLZO. One of the reasons for this behaviour could be that the higher content of LLZO filler (95 wt%) lowers the T_g values of the polymers.[35] A second trend of decreasing T_g values was seen with molecular weight of PEO present in the matrix of the separators with 95 wt% of LLZO: PEO1000k < PEO600k < PEO300k. Separators prepared with different LLZO content (43 wt%, 90 wt% and 95 wt%) and PEO with same molecular weight of 600 kg/mol were also compared, the T_g values for these three separators was found to slightly decrease with increasing LLZO content. This shows the correlation between the decrease in T_g for polymers and addition of ceramic fillers in SCEs.

Separators with 90 wt% of LLZO prepared with PEO1000k and PEO300k (LZ90_PEO1000k and LZ90_PEO300k) exhibited higher crystallinity values (Figure 4a), compared to separators with 95 wt% of LLZO with the same PEO molecular weights.

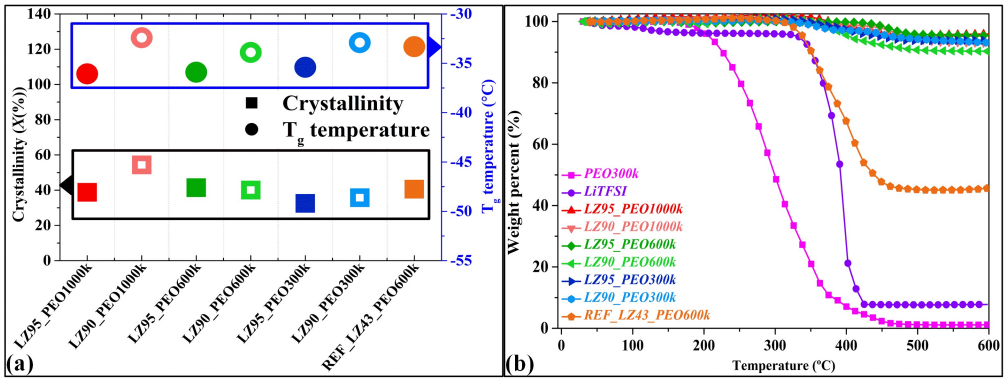

Figure 4. (a) Graphs showing the crystallinity (rectangle points) and T_g (circular points) of the prepared INURSE separators; (b) TGA traces for PEO300k, LiTFSI, and prepared separators – INURSE and reference.

The observation of increased crystallization values for LZ90_PEO1000k and LZ90_PEO300k separators can be associated to the higher weight fraction of PEO present in the composition compared to separators with 95 wt% of LLZO. The higher weight fraction of PEO translates to high volume fraction in the separators which could cause aggregation of the polymeric matrix in some areas of the microstructure giving rise to higher crystallinity values. This behaviour was also similarly reported by X. Mei *et al.*,[36] where they observed high crystallinity values for composite films prepared with high content of ceramic due to spatial arrangement of LLZO particles. The cross-sectional microstructure; LZ90_PEO1000k – Figure S5d and LZ90_PEO300k – Figure 3g; shows fewer pores, which could contribute to higher crystallinity values. DSC traces of the investigated composite separators can be found in *Supplementary Information* (Figure S4).

The separators with 95 wt% content of LLZO increases the surface area of LLZO particles in the separators to interact with the polymeric matrix, which could decrease of the crystallinity of PEO. Another factor in the reduction of crystallinity of separators with 95 wt% LLZO could be the presence of pores in its structure. The pores are clearly visible in LZ95_PEO1000k (Figure 3e), but not in LZ90_PEO1000k (Figure S5d). Li *et al.*, reported that a large number of pores in the polymer matrix[37] also reduces the crystallinity of PEO in composite separators. However, anomalous behaviour was observed in separators prepared with PEO600k. LZ90_PEO600k (90 wt% LLZO) showed a slightly lower crystallinity compared to LZ95_PEO600k (95 wt% LLZO). This behaviour contradicts the knowledge that a higher fraction of ceramics lowers the crystallinity of polymer matrix. There could be several reasons for this increased crystallinity, such as agglomeration of LLZO particles due to high content of ceramics[38] and the different particle size distribution of the LLZO powder used to make the separator.[39]

Figure 4b shows the TGA curves for PEO, LiTFSI and all separators (INURSE and reference) investigated in this study. The curves show that residue of all INURSE separators at 600°C are greater than 90 wt%, confirming the presence of LLZO in target amounts. This also shows the excellent thermal stability of composite separator with ceramic residue, which will lead to better operational safety of final SSB. Interestingly, it shows that the decomposition of PEO and LiTFSI is shifted to higher temperatures (more than 390 °C) at high LLZO content. The thermal decomposition of reference electrolyte is influenced by LiTFSI, with decomposition temperature being in the same range.

2.3. Electrical Properties

The EIS measurements for all INURSE separators were performed between 80 °C and 30 °C. REF_LZ43_PEO600k separator was also tested to understand the influence of the amount of LLZO on the ionic conductivity.

Figure 5a shows the temperature dependence of ionic conductivity for all prepared composite separators. In the case of INURSE separators, ionic conductivity values was found to increase with decreasing molecular weight (PEO1000k < PEO600k < PEO300k). Low ionic conductivity values for PEO1000k based separators (LZ95_PEO1000k and LZ90_PEO1000k) could be due to higher number of entanglements and other interaction within polymer chains with higher molecular weights that would hinder ion transport.[40] It should also be noted that pores present in both electrolytes (LZ95_PEO1000k — Figure S5b and LZ90_PEO1000k – Figure S5d) would adversely affect conductivity values. All INURSE separators were found to have lower ionic conductivity (by an order of magnitude) compared to REF_LZ43_PEO600k separator. This suggests that the increased amount of PEO-LiTFSI in matrix of REF_LZ43_PEO600k provides more pathways for Li-ion conduction.[17] The low ionic conductivity of INURSE separators could be due to several reasons, such as lack of conduction pathways due to the small volume of PEO-LiTFSI phase, high tortuosity (as seen in Figure 3e and Figure 3g) and absence of efficient Li-ion exchange at the interfaces between PEO-LiTFSI matrix and LLZO particles.[41]

To investigate the influence of addition of Li-ion conducting LLZO and inert Al_2O_3 fillers at high ceramic content in composite separators, REF_$Al_2O_3$90_PEO600k separator was also fabricated and investigated. REF_$Al_2O_3$90_PEO600k separator

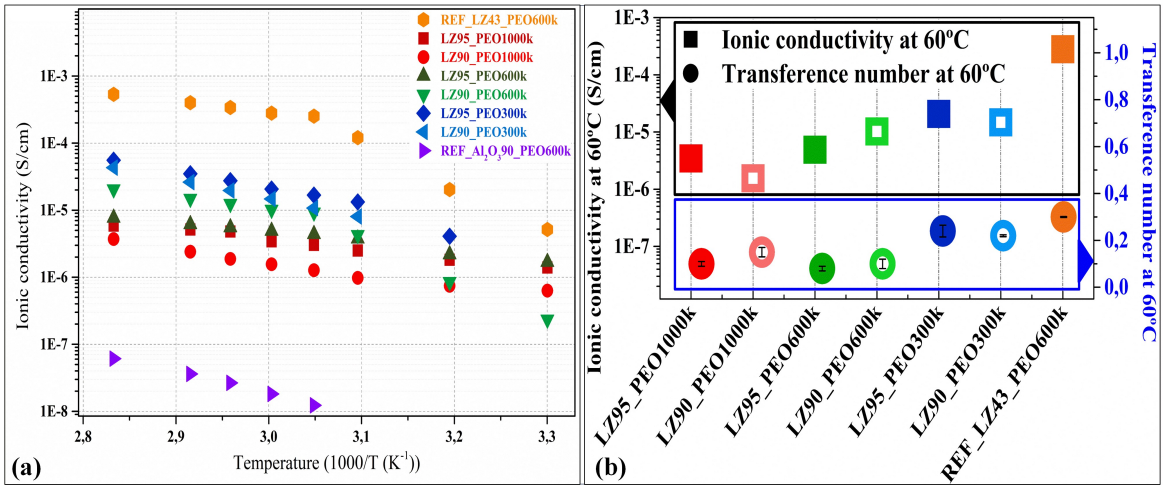

Figure 5. (a) Temperature-dependent ionic conductivity values for all INURSE separators; (b) Conductivity values (square symbol) at 60 °C and calculated transference number (circle symbol) for all INURSE separators.

shows ionic conductivity of 1.82×10^{-8} S/cm at 60 °C, which is much lower than the conductivity of the worst INURSE separators with lowest ionic conductivity of 1.55×10^{-6} S/cm at 60 °C.

Both trends in INURSE separators show that LLZO improves ionic conductivity, but its contribution to conductivity at frequencies that affect the overall conductivity of the separators is effectively slow. Ranque *et al.*[42] and Ghorbanzade *et al.*[43] observed with ^{7}Li-^{7}Li 2D exchange (EXSY) solid-state NMR spectra that the time scale of Li ion exchange between LLZO and the polymer matrix is very long. A similar behaviour of LLZO in the polymer matrix was also observed by Lechartier *et al.*,[44] who reported using SS-NMR, that the mobility of Li cations in polymer phase decreases with increasing LLZO content.

As already mentioned, properties and behaviour of composite separators with such high ceramic contents are similar to those of respective ceramics. Therefore, it can be assumed that the ceramic-rich composite separators produced with inert fillers such as Al_2O_3 exhibit insulating behaviour. In contrast, ionic conductivity of ceramic-rich CSEs containing LLZO were up to four orders of magnitude higher, which is due to the intrinsically high Li-ion conductivity of the LLZO.

Since all electrochemical tests were to be conducted at 60 °C, we were interested in conductivity values and behaviour at 60 °C. Figure S6a shows the Nyquist plot for impedance spectra for all separators at 60 °C with the equivalent circuit used to fit the data. Equivalent circuit shown in the figure consists of R1- representing bulk resistance, R2 || CPE2- representing the semicircle indicative of charge transfer and electrolyte-electrode interface and CPE1- representing the ion-blocking electrodes. Highest ionic conductivity values at 60 °C were observed for LZ95_PEO300k, LZ90_PEO300k and REF_LZ43_PEO600k with 2.06×10^{-5} S/cm, 1.47×10^{-5} S/cm and 2.79×10^{-4} S/cm, respectively. Slightly higher ionic conductivity values were observed for separators with 95 wt% LLZO (LZ95_PEO1000k and LZ95_PEO300k), which could be attributed to lower T_g values[35] and decreased crystallinity values.[15] It could also be due to LLZO/PEO-LiTFSI interface being slightly more exposed, which could prompt the formation of space-charge regions[45–46] which could be promoting an increase in ionic conductivity values in separators with 95 wt% LLZO compared to 90 wt%. However, in the case of PEO600k – LZ95_PEO600k and LZ90_PEO600k separators, the observed inverse behaviour could be explained by the incompatibility between PEO-LiTFSI matrix and LLZO during processing. This anomalous behaviour was similar to that observed during analysis of T_g values (Figure 4a).

Upon polarization of symmetric Li/LZ90_PEO300k/Li cell, the current was stabilised after 6 h (Figure S6c). Figure S6b shows the original EIS spectra before and after cell polarization and their fits using equivalent circuit in Figure S6d. It was observed that separators prepared with higher molecular weight PEO have relatively low transference numbers as seen in Figure 5b. This was also reported by Timachova *et al.*,[47] who showed that ionic motion in electrolytes with molecular weight higher than 10^4 g/mol occurs by segmental motion. This type of behaviour apparently applies also for INURSE separators, as shown in Figure 5b, where transference numbers for INURSE and REF separators at 60 °C are in the range of 0.08–0.12. In the case of LZ95_PEO300k and LZ90_PEO300k, higher transference numbers of 0.24 and 0.22, respectively, were determined. LZ95_PEO600k and LZ90_PEO600k showed transference number of 0.08 and 0.1. All the latter values are well below t^+ value of 0.3[31] for REF_LZ43_PEO600k, demonstrating the importance of PEO with relatively low Mw for the development of INURSE electrolytes.

2.4. Electrochemical Properties

Symmetric Li/Li coin cells were used for assessment of the prepared composite separators for their stability with Li metal and the ability to resist the growth of Li dendrites.[48] The initial

evaluation of symmetric Li/Li coin cells with INURSE and reference separators with galvanostatic cycling was carried out at a low current density (CD) of 0.01 mA/cm^2 with 1 h step. The low CD value was chosen, considering the low ionic conductivity for INURSE separators. Figure S8 shows the voltage vs time profiles for Li stripping-plating behaviour in symmetric Li/Li cells of all prepared separators. Symmetric Li/Li cells with INURSE separators: LZ95_PEO1000k, LZ95_PEO600k, LZ90_PEO600k and REF_LZ43_PEO600k, showed similar behaviour of increased polarization at start of cycling. The decrease in polarization observed during later cycles could be attributed to several reasons. One of them could be the increase of electrode surface area because of plating of high surface area Li, which may indirectly help in preventing a concentrated Li deposition at points of Li seeding on the foil during cycling.[49]

It should be noted that REF_LZ43_PEO600k, LZ90_PEO300k and LZ95_PEO300k separators were selected for all further electrochemical characterizations at 60 °C after analysis of the ionic conductivity, Li transference number values and the polarization values of symmetric Li/Li cells at 0.01 mA/cm^2. First, critical current density (CCD) test[50–51] was performed on REF_LZ43_PEO600k, LZ90_PEO300k and LZ95_PEO300k separators (Figure 6a) to further understand Li stripping/plating behaviour. Symmetric Li/Li cells with REF_LZ43_PEO600k, LZ90_PEO300k and LZ95_PEO300k separators exhibited stability for current densities until 0.1 mA/cm^2, 0.25 mA/cm^2 and 0.5 mA/cm^2, respectively. It was observed that based on the amount of LLZO present in matrix, INURSE separators endured galvanostatic cycling until higher current densities. From the relatively high CCD value for LZ95_PEO300k, it could be ascertained that separators with high amount of LLZO could sustain higher CDs by accommodation of lithium deposit in a porous (scaffold-like) structure typical for ceramic-rich separators.[52] Figure S7 compares the cycling performance of LZ90_PEO300k and LZ95_PEO300k at high CD of 0.2 mA/cm^2, where it was also congruently observed that Li/Li cells with LZ95_PEO300 K showed higher stability during cycling against dendrites formation and propagation through the separators.

To confirm CD values obtained for LZ90_PEO300k and LZ95_PEO300k INURSE separators, long-term cycling of symmetric Li/Li cells at a higher and realistic current density value of 0.1 mA/cm^2 were performed. The stable polarization of LZ90_PEO300k based cell shows excellent separator compatibility with Li metal even at the higher current densities as observed in Figure 6b. Even though a higher CCD value seen for LZ95_PEO300k, but this has not translated into long-term cycling stability, which is apparent from the increasing polarization during cycling. As mentioned earlier during CCD testing, LZ95_PEO300k showed stability at higher CDs probably due to the porous structure. However, during long term cycling, the accommodated Li could create a tortuous patch for fresh Li to be plated/stripped, hence showing increasing polarization.[53]

Figure S9 depicts the impedance spectra of Li/Li cells upon aging at 60 °C with LZ90_PEO300k and LZ95_PEO300k separators. Symmetric Li/Li cells with LZ95_PEO300k showed higher impedance compared to LZ90_PEO300k. However, there was only a slight change in the impedance spectra of Li/Li cells for both separators over the testing period, showing formation of stable Li/INURSE interface. Figure S13 depicts the surface and cross-sectional SEM images of the Li/Li cell with LZ90_PEO300k separator disassembled after long-term cycling for post-mortem analysis (PMA). SEM images of cross-section (Figures S13 a–c), exhibit good interfacial contact between lithium foil and INURSE separator. In Figures S13 e and S13 f, two types of lithium deposition were observed, dense layered columnar type of structure in most of the areas and in few regions some of the deposits which have a tubular and compact structure.

To further understand and assess electrochemical properties of INURSE and reference separators under realistic operational conditions, galvanostatic cycling of full cells with Li metal anode and NMC622 based composite cathode was performed. Figure S10 shows results from the floating test assessing electrochemical stability limits for the three investigated separators. The stability limit for investigated separators, REF_LZ43_PEO600k, LZ90_PEO300k and LZ95_PEO300k are seen to be 4.3 V, 4.6 V and 4.8 V, respectively. These results demonstrate

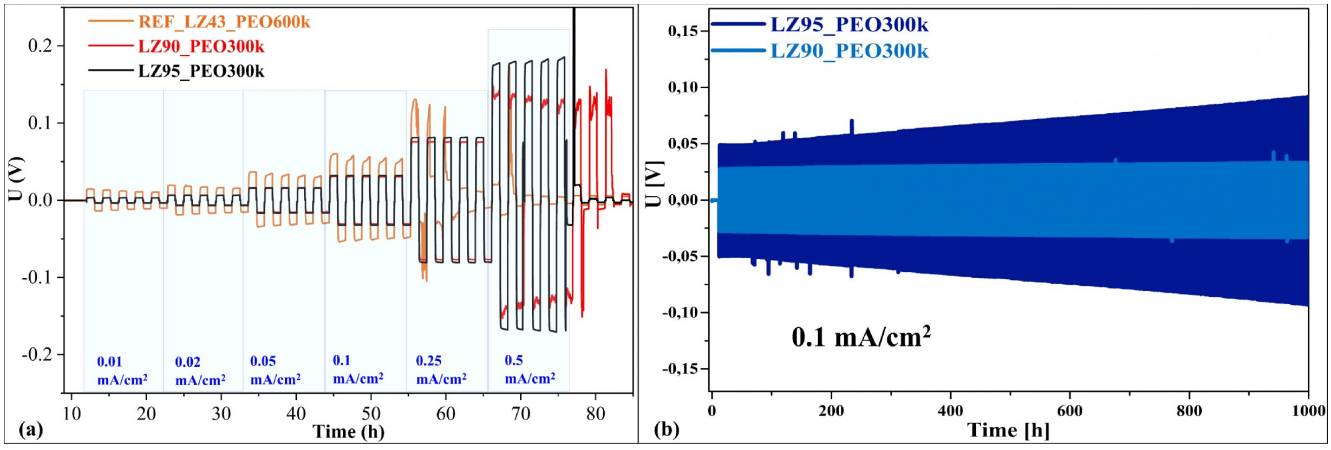

Figure 6. (a) Critical current density test: voltage versus time profiles for symmetric Li/Li cells for REF_LZ43_PEO600k, LZ90_PEO300k and LZ95_PEO300k; (b) Voltage versus time profiles for symmetric Li/Li cells with LZ90_PEO300k and LZ95_PEO300k at current density of 0.1 mA/cm^2 and 1 h step. All measurements were performed at 60 °C.

that electrochemical oxidative stability of the INURSE separators is highly depended on the content of LLZO in the matrix.

Solid-state coin cells were assembled with REF_LZ43_PEO600k and INURSE separators (LZ95_PEO600k, LZ90_PEO600k, LZ95_PEO300k and LZ90_PEO300k), in "Li/separator/NMC622" format. The assembly procedure (Figure S3) for coin cells is detailed in *Supplementary Information*. Figure 7a depicts the cyclability of solid-state Li/NMC622 coin cells cycled at 0.05 C/0.1D and 60 °C within 3.0–4.3 V interval. The initial discharge capacities of solid-state cells with INURSE and reference separators are as follows: REF_LZ43_PEO600k – 182 mAh/g, LZ95_PEO600k – 44 mAh/g, LZ90_PEO600k – 122 mAh/g, LZ95_PEO300k – 126 mAh/g and LZ90_PEO300k – 163 mAh/g, respectively. The initial discharge capacities decreased on increase of ceramic filler amount. The highest discharge capacity was observed in REF_LZ43_PEO600k with 43 wt% of LLZO compared to INURSE separators with 90 wt% and 95 wt% of LLZO. With INURSE separators (i) cells with separators having lower ceramic content (90 wt% > 95 wt%) showed higher discharge capacities for same molecular weight of PEO and (ii) cells with low molecular weight PEO based separators showed higher discharge capacities (PEO300k > PEO600k) for the same ceramic content. Figure 7b depict voltage versus capacity curves for 1st and 10th cycles of the cells with REF_LZ43_PEO600k and LZ90_PEO300k separators cycled within 3.0–4.3 V interval.

Figure S11 a shows the cyclability of the solid-state coin cells assembled with REF_LZ43_PEO600k and LZ90_PEO300k, cycled within voltage range of 3.0–4.2 V, also at 0.05 C/0.1D and 60 °C. The initial discharge capacity for cells with both separators are REF_LZ43_PEO600k – 172 mAh/g, and LZ90_PEO300k – 132 mAh/g, respectively. As expected, the discharge capacities observed in the cells with LZ90_PEO300k charged until 4.2 V are lower comparing to 4.3 V due to charging to a lower cut-off voltage. Similar trend is seen with the cells assembled with REF_LZ43_PEO600k. It was seen that when cycling was done within 3.0–4.2 V range, the rate of capacity fade was lower with higher coulombic efficiency. The relevant initial discharge capacities achieved in solid-state cells with REF_LZ43_PEO600k could be attributed to the higher ionic conductivity of composite separator and lower interfacial resistance caused by better wetting of electrodes by polymer-rich solid electrolyte. It was observed that the discharge capacity fade after 10 cycles for cells with both separators was significant in both cycling intervals. However, a trend can be seen with both separators showing capacity fade at a similar rate in both cycling intervals. Figure S11 b depict the voltage versus capacity curves for 1st and 10th cycles of the cells with REF_LZ43_PEO600k and LZ90_PEO300k separators cycled within 3.0–4.2 V interval. In both cases, cells with REF_LZ43_PEO600k separator demonstrated lower polarization.

Figure S11 c and Figure S11 d show voltage versus normalized capacity curves for 1st and 10th cycles of cells cycled with REF_LZ43_PEO600k and LZ90_PEO300k separators in 3.0–4.3 V and 3.0–4.2 V intervals, respectively. The build-up of resistance in the cells, can be observed by the drop in the voltage in the initial part of the discharge curve for the 10th cycle for both separators as depicted in Figure S11 c. The observed resistance build-up could be attributed to decomposition of the PEO based polymeric matrix in both cathode and separator. In 3.0–4.2 V range in Figure S11 d for both separators, the initial drop in the cell voltage while discharging from 4.2 V is comparatively lower in the 10th cycle which shows there is less build-up of resistance.

Figure 8 and Figure S12 depict the incremental capacity (dQ/dV) curves for the tested cells. In all cases, there is reduction of intensity in both cathodic and anodic peaks for the 10th cycle compared to that of the 1st cycle. There were no additional peaks observed in all the dQ/dV curves, which could indicate that PEO decomposition is hidden by electrochemical signal of NMC622 electrode. The broadening of peaks upon cycling is more pronounced for LZ90_PEO300k cells comparing to REF_LZ43_PEO600k ones. Such behaviour could be seen due to the overall increase of internal cell resistance observed in Figure S11. The other features observed are changes in the kinetic limitations could be attributed to the anodic peak shift (increase in Ohmic resistance).[54]

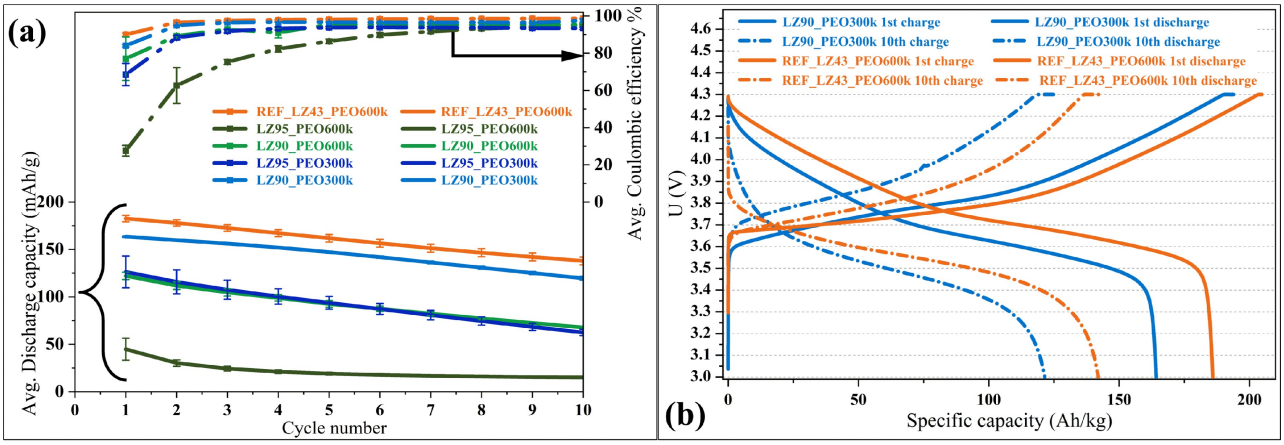

Figure 7. (a) Discharge capacity and coulombic efficiency for Li/NMC622 solid-state cells cycled under 0.05 C/0.1D at 60 °C within cycling range of 3.0–4.3 V. (b) Voltage vs specific capacity profiles for 1st and 10th cycle for cell cycled within 3.0–4.3 V.

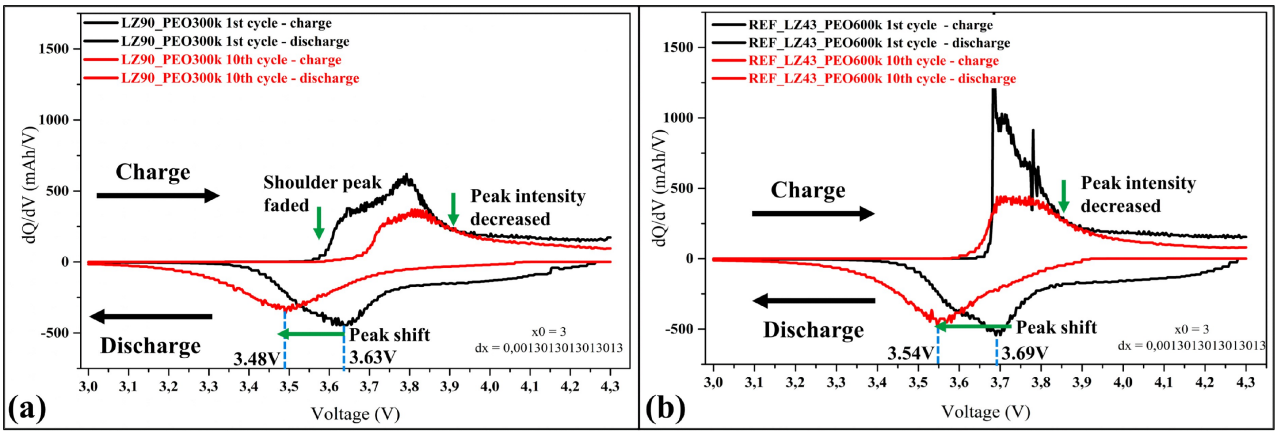

Figure 8. dQ/dV curves for cell charged up to 4.3 V - (a) LZ90_PEO300k (b) REF_LZ43_PEO600k.

Thus, even with drastic decrease of PEO content in the investigated ceramic-rich separators, electrochemical performance of Li/NMC622 solid state cells cycled at 60 °C did not improve. Therefore, for next phase of study, we will try to design INURSE separators using polymer hosts stable to electro-oxidation at electrode potential >4.0 V vs Li/Li^+. As part of future work, we will further study and cycle these separators in full cells with $LiFePO_4$ (LFP) based cathode, to understand their behaviour with low-voltage cathodes.

3. Conclusions

In this work, INURSE composite separators with ultra-high content of 90 wt% and 95 wt% ceramic LLZO in the PEO-LiTFSI matrix have been successfully fabricated and investigated as a model composite electrolyte system.

Due to easy processability of the polymer component, separators have been prepared in a simple and easily scalable process using standard equipment. The simple manufacturing process gives the INURSE separators various advantages over solid inorganic separators, which must be sintered at high temperatures and are difficult to scale up to industrial cell sizes. Although polymer content in the separators is very low, they can maintain good mechanical flexibility. Free-standing separators with satisfactory thermal stability have been successfully produced with PEO of different molecular weights (300, 600 and 1,000 kg/mol). However, separators with a molecular weight of 100 kg/mol encountered problems in the formation of self-standing films.

INURSE separators prepared with PEO300k (LZ90_PEO300k) exhibited higher ionic conductivity (1.4×10^{-5} S/cm at 60 °C) compared to other INURSE separators. INURSE separators based on LLZO as an active filler clearly showed higher ion conductivity compared to separators prepared with a passive filler such as Al_2O_3. Thus, our study clearly shows that for practical realization of ceramic-rich composite separators, active inorganic fillers that conduct Li cations should be used instead of passive insulating fillers.

LZ90_PEO300k separator proved to be stable in a contact with the Li metal anode during storage at 60 °C. Li/Li cells with LZ90_PEO300k separator withstood critical current density until 0.25 mA/cm^2 during the CCD test. Additionally, Li/LZ90_PEO300k/Li cell showed stable polarization at 0.1 mA/cm^2 during long-term cycling for 1000 h due to formation of uniform plated lithium with dense morphology.

In turn, Li/LZ90_PEO300k/NMC622 coin cells showed relevant discharge capacity in the 1st cycle but slightly lower than for reference REF_LZ43_PEO600k separator. However, the capacity retention of Li/NMC622 cells with LZ90_PEO300k was seen to be similar to that of the cells with the reference separator. There were no improvements or increase seen in capacity retention even with the addition of high content of ceramics to the system. This lack of improvement could be attributed to rapid build-up of internal cell resistance probably related to breakdown of the PEO polymer matrix in either separator or cathode.

It is important to note that compared to pressure applied to cells with SIE separators, INURSE separators have been tested in Li/Li and Li/NMC622 coin cells without any additional pressure applied which is clear advantage comparing to solid state cells equipped with LLZO-based ceramic separators.

In summary, LZ90_PEO300k separator with 90 wt% of LLZO in a matrix with LiTFSI and PEO with Mw of 300,000 g/mol exhibited the best performance among studied ones. It has been demonstrated that the processability and performance of investigated solid composite separators with high active filler contents strongly depended on the molecular weight of PEO used in the matrix.

Taking into account the results reported in this study, future work on ceramic-rich composite systems should therefore focus on improving and optimizing polymer matrix, particularly with regard to stability towards high-voltage cathode materials and lowering cell operating temperature to ambient temperature.

Acknowledgements

KV acknowledges funding from the DESTINY COFUND PhD Programme which has received funding from European Union's Horizon 2020 research and innovation programme under the Marie Sklodowska-Curie (grant agreement No 945357) and Fundación CIDETEC. Financial support from the German "Federal Ministry of Education and Research" (BMBF) under grant numbers 13XP0434 A (FestBatt 2 – Oxid) and 13XP0428 A (FestBatt 2 – Hybride) is gratefully acknowledged. The authors also gratefully acknowledge Grit Häuschen and Philipp Hecker from Forschungszentrum Jülich GmbH for help with synthesis of LLZO powders used in this work. Authors would also like to acknowledge Iratxe de Meatza for assistance with XRD measurements, Dr Aratz Genua for assistance with TGA measurements, Dr Sarah Montes for assistance with DSC measurements and Dr Izaskun Combarro for assistance with FE-SEM (all from CIDETEC). Open Access funding enabled and organized by Projekt DEAL.

Conflict of Interests

The authors declare no conflict of interest.

Data Availability Statement

The data that support the findings of this study are available from the corresponding author upon reasonable request.

Keywords: Solid composite electrolyte · ceramic-rich composite separator · lithium metal battery · solid state batteries

[1] M. Ghalkhani, S. Habibi, in *Energies, Vol. 16*, **2023**.
[2] M. Armand, P. Axmann, D. Bresser, M. Copley, K. Edström, C. Ekberg, D. Guyomard, B. Lestriez, P. Novák, M. Petranikova, W. Porcher, S. Trabesinger, M. Wohlfahrt-Mehrens, H. Zhang, *J. Power Sources* **2020**, *479*, 228708.
[3] L. Wang, J. Ma, C. Wang, X. Yu, R. Liu, F. Jiang, X. Sun, A. Du, X. Zhou, G. Cui, *Adv. Sci.* **2019**, *6*, 1900355.
[4] G. Liang, Z. Wu, C. Didier, W. Zhang, J. Cuan, B. Li, K.-Y. Ko, P.-Y. Hung, C.-Z. Lu, Y. Chen, G. Leniec, S. M. Kaczmarek, B. Johannessen, L. Thomsen, V. K. Peterson, W. K. Pang, Z. Guo, *Angew. Chem. Int. Ed.* **2020**, *59*, 10594–10602.
[5] H. Darjazi, E. Gonzalo, B. Acebedo, R. Cid, M. Zarrabeitia, F. Bonilla, M. Á. Muñoz-Márquez, F. Nobili, *Mater. Today* **2022**, *20*, 100236.
[6] J. Janek, W. G. Zeier, *Nat. Energy* **2016**, *1*, 16141.
[7] A. Varzi, R. Raccichini, S. Passerini, B. Scrosati, *J. Mater. Chem. A* **2016**, *4*, 17251–17259.
[8] G. Rollo-Walker, N. Malic, X. Wang, J. Chiefari, M. Forsyth, in *Polymers, Vol. 13*, **2021**.
[9] S. Huo, L. Sheng, W. Xue, L. Wang, H. Xu, H. Zhang, X. He, *InfoMat* **2023**, *5*, e12394.
[10] Y. Liang, H. Liu, G. Wang, C. Wang, Y. Ni, C.-W. Nan, L.-Z. Fan, *InfoMat* **2022**, *4*, e12292.
[11] R. Pacios, A. Villaverde, M. Martínez-Ibañez, M. Casas-Cabanas, F. Aguesse, A. Kvasha, *Adv. Energy Mater.* **2023**, *13*, 2301018.
[12] M. Keller, G. B. Appetecchi, G.-T. Kim, V. Sharova, M. Schneider, J. Schuhmacher, A. Roters, S. Passerini, *J. Power Sources* **2017**, *353*, 287–297.
[13] C. Wang, Y. Yang, X. Liu, H. Zhong, H. Xu, Z. Xu, H. Shao, F. Ding, *ACS Appl. Mater. Interfaces* **2017**, *9*, 13694–13702.
[14] X. Zhu, K. Wang, Y. Xu, G. Zhang, S. Li, C. Li, X. Zhang, X. Sun, X. Ge, Y. Ma, *Energy Storage Mater.* **2021**, *36*, 291–308.
[15] X. Yang, J. Liu, N. Pei, Z. Chen, R. Li, L. Fu, P. Zhang, J. Zhao, *Nano-Micro Lett.* **2023**, *15*, 74.
[16] G. M. Overhoff, M. Y. Ali, J.-P. Brinkmann, P. Lennartz, H. Orthner, M. Hammad, H. Wiggers, M. Winter, G. Brunklaus, *ACS Appl. Mater. Interfaces* **2022**, *14*, 53636–53647.
[17] L. Chen, Y. Li, S.-P. Li, L.-Z. Fan, C.-W. Nan, J. B. Goodenough, *Nano Energy* **2018**, *46*, 176–184.
[18] H. Al-Salih, M. Cui, C.-H. Yim, Z. Sadighi, S. Yan, Z. Karkar, G. R. Goward, E. A. Baranova, Y. Abu-Lebdeh, *J. Electrochem. Soc.* **2022**, *169*, 080510.
[19] J.-H. Choi, C.-H. Lee, J.-H. Yu, C.-H. Doh, S.-M. Lee, *J. Power Sources* **2015**, *274*, 458–463.
[20] Q. Guo, Y. Han, H. Wang, S. Xiong, Y. Li, S. Liu, K. Xie, *ACS Appl. Mater. Interfaces* **2017**, *9*, 41837–41844.
[21] D. Cai, D. Wang, Y. Chen, S. Zhang, X. Wang, X. Xia, J. Tu, *Chem. Eng. J.* **2020**, *394*, 124993.
[22] D. H. Kim, M. Y. Kim, S. H. Yang, H. M. Ryu, H. Y. Jung, H.-J. Ban, S.-J. Park, J. S. Lim, H.-S. Kim, *J. Ind. Eng. Chem.* **2019**, *71*, 445–451.
[23] Z. Huang, W. Pang, P. Liang, Z. Jin, N. Grundish, Y. Li, C.-A. Wang, *J. Mater. Chem. A* **2019**, *7*, 16425–16436.
[24] W. Zha, F. Chen, D. Yang, Q. Shen, L. Zhang, *J. Power Sources* **2018**, *397*, 87–94.
[25] S. Yu, Q. Xu, X. Lu, Z. Liu, A. Windmüller, C.-L. Tsai, A. Buchheit, H. Tempel, H. Kungl, H.-D. Wiemhöfer, *ACS Appl. Mater. Interfaces* **2021**, *13* (51), 61067–61077
[26] T. Jiang, P. He, G. Wang, Y. Shen, C.-W. Nan, L.-Z. Fan, *Adv. Energy Mater.* **2020**, *10*, 1903376.
[27] Y.-C. Jung, M.-S. Park, C.-H. Doh, D.-W. Kim, *Electrochim. Acta* **2016**, *218*, 271–277.
[28] J. Bae, Y. Li, F. Zhao, X. Zhou, Y. Ding, G. Yu, *Energy Storage Mater.* **2018**, *15*, 46–52.
[29] J. H. Cha, P. N. Didwal, J. M. Kim, D. R. Chang, C.-J. Park, *J. Membr. Sci.* **2020**, *595*, 117538.
[30] M.-S. Park, Y.-C. Jung, D.-W. Kim, *Solid State Ionics* **2018**, *315*, 65–70.
[31] T. Thieu, E. Fedeli, O. Garcia-Calvo, I. Combarro, J. Nicolas, I. Urdampilleta, A. Kvasha, *Electrochim. Acta* **2021**, *397*, 139249.
[32] Q. Guo, F. Xu, L. Shen, S. Deng, Z. Wang, M. Li, X. Yao, *Energy Material Advances, 2022*.
[33] K. W. Ebagninin, A. Benchabane, K. Bekkour, *J. Colloid Interface Sci.* **2009**, *336*, 360–367.
[34] R. P. Wool, *Macromolecules* **1993**, *26*, 1564–1569.
[35] J. Fu, Z. Li, X. Zhou, X. Guo, *Materials Advances* **2022**, *3*, 3809–3819.
[36] X. Mei, Y. Wu, Y. Gao, Y. Zhu, S.-H. Bo, Y. Guo, *Materials Today Communications* **2020**, *24*, 101004.
[37] X. Li, S. Liu, J. Shi, M. Huang, Z. Shi, H. Wang, Z. Yan, *Chem. Eng. J.* **2023**, *468*, 143795.
[38] C. Yan, P. Zhu, H. Jia, Z. Du, J. Zhu, R. Orenstein, H. Cheng, N. Wu, M. Dirican, X. Zhang, *Energy Storage Mater.* **2020**, *26*, 448–456.
[39] D. Hwang, M.-Y. Kim, Y.-W. Song, L. HyoChan, S.-J. Kim, B.-s. Kang, Y. Hong, H.-s. Kim, J. Kim, J. Lim, *Solid State Ionics* **2023**, *397*, 116245.
[40] J. Shi, C. A. Vincent, *Solid State Ionics* **1993**, *60*, 11–17.
[41] F. P. Nkosi, M. Valvo, J. Mindemark, N. A. Dzulkurnain, G. Hernández, A. Mahun, S. Abbrent, J. Brus, L. Kobera, K. Edström, *ACS Appl. Energ. Mater.* **2021**, *4*, 2531–2542.
[42] P. Ranque, J. Zagórski, S. Devaraj, F. Aguesse, J. M. López del Amo, *J. Mater. Chem. A* **2021**, *9*, 17812–17820.
[43] P. Ghorbanzade, G. Accardo, K. Gomez, P. López-Aranguren, S. Devaraj, C. M. Costa, S. Lanceros-Mendez, J. M. López del Amo, *Mater. Today* **2023**, *38*, 101448.
[44] M. Lechartier, L. Porcarelli, H. Zhu, M. Forsyth, A. Guéguen, L. Castro, D. Mecerreyes, *Materials Advances* **2022**, *3*, 1139–1151.
[45] Z. Li, H.-M. Huang, J.-K. Zhu, J.-F. Wu, H. Yang, L. Wei, X. Guo, *ACS Appl. Mater. Interfaces* **2019**, *11*, 784–791.
[46] Z. Li, J. Fu, X. Zhou, S. Gui, L. Wei, H. Yang, H. Li, X. Guo, *Adv. Sci.* **2023**, *10*, 2201718.
[47] K. Timachova, H. Watanabe, N. P. Balsara, *Macromolecules* **2015**, *48*, 7882–7888.
[48] J. Xiao, Q. Li, Y. Bi, M. Cai, B. Dunn, T. Glossmann, J. Liu, T. Osaka, R. Sugiura, B. Wu, J. Yang, J.-G. Zhang, M. S. Whittingham, *Nat. Energy* **2020**, *5*, 561–568.
[49] G. Bieker, M. Winter, P. Bieker, *Phys. Chem. Chem. Phys.* **2015**, *17*, 8670–8679.
[50] S. Sarkar, V. Thangadurai, *ACS Energy Lett.* **2022**, *7*, 1492–1527.

[51] H. Shen, E. Yi, L. Cheng, M. Amores, G. Chen, S. W. Sofie, M. M. Doeff, *Sustain. Energy Fuels* **2019**, *3*, 1647–1659.
[52] F. Okur, H. Zhang, D. T. Karabay, K. Muench, A. Parrilli, A. Neels, W. Dachraoui, M. D. Rossell, C. Cancellieri, L. P. H. Jeurgens, K. V. Kravchyk, M. V. Kovalenko, *Adv. Energy Mater.* **2023**, *13*, 2203509.
[53] K.-H. Chen, K. N. Wood, E. Kazyak, W. S. LePage, A. L. Davis, A. J. Sanchez, N. P. Dasgupta, *J. Mater. Chem. A* **2017**, *5*, 11671–11681.
[54] M. Dubarry, D. Anseán, *Front. Energy Res.* **2022**, *10*.
[55] M. Mann, M. Küpers, G. Häuschen, M. Finsterbusch, D. Fattakhova-Rohlfing, O. Guillon, *Ionics* **2022**, *28*, 53–62.
[56] R. Murugan, V. Thangadurai, W. Weppner, *Angew. Chem. Int. Ed.* **2007**, *46*, 7778–7781.
[57] J. Awaka, N. Kijima, H. Hayakawa, J. Akimoto, *J. Solid State Chem.* **2009**, *182*, 2046–2052.
[58] X. Tong, V. Thangadurai, E. D. Wachsman, *Inorg. Chem.* **2015**, *54*, 3600–3607.
[59] H. Huo, J. Luo, V. Thangadurai, X. Guo, C.-W. Nan, X. Sun, *ACS Energy Lett.* **2020**, *5*, 252–262.
[60] S. A. Yoon, N. R. Oh, A. R. Yoo, H. G. Lee, H. C. Lee, *J. Korean Ceram. Soc.* **2017**, *54*, 278–284.
[61] P. Ghorbanzade, A. Pesce, K. Gómez, G. Accardo, S. Devaraj, P. López-Aranguren, J. M. López del Amo, *J. Mater. Chem. A* **2023**, *11*, 11675–11683.
[62] J. Zagórski, J. M. López del Amo, M. J. Cordill, F. Aguesse, L. Buannic, A. Llordés, *ACS Appl. Energ. Mater.* **2019**, *2*, 1734–1746.
[63] A. I. Waidha, T. Ferber, M. Donzelli, N. Hosseinpourkahvaz, V. Vanita, K. Dirnberger, S. Ludwigs, R. Hausbrand, W. Jaegermann, O. Clemens, *ACS Appl. Mater. Interfaces* **2021**, *13*, 31111–31128.
[64] V. Vanita, A. I. Waidha, S. Yadav, J. J. Schneider, O. Clemens, *Int. J. Appl. Ceram. Technol.* **2023**, *20*, 236–250.
[65] P. Ghorbanzade, G. Accardo, K. Gomez, P. López-Aranguren, S. Devaraj, C. M. Costa, S. Lanceros-Mendez, J. M. López del Amo, *Mater. Today* **2023**, *38*, 101448.
[66] Z. Huang, W. Pang, P. Liang, Z. Jin, N. Grundish, Y. Li, C.-A. Wang, *J. Mater. Chem. A* **2019**, *7*, 16425–16436.
[67] J. Wu, X. Wu, W. Wang, Q. Wang, X. Zhou, Y. Liu, B. Guo, *RSC Adv.* **2020**, *10*, 22417–22421.
[68] Q. Guo, F. Xu, L. Shen, S. Deng, Z. Wang, M. Li, X. Yao, *Energy Material Advances* **2022**.
[69] F. P. Nkosi, M. Valvo, J. Mindemark, N. A. Dzulkurnain, G. Hernández, A. Mahun, S. Abbrent, J. Brus, L. Kobera, K. Edström, *ACS Appl. Energ. Mater.* **2021**, *4*, 2531–2542.
[70] T. Jiang, P. He, G. Wang, Y. Shen, C.-W. Nan, L.-Z. Fan, *Adv. Energy Mater.* **2020**, *10*, 1903376.
[71] H. Liu, J. Li, W. Feng, G. Han, *Ionics* **2021**, *27*, 3339–3346.
[72] C. Wang, Y. Yang, X. Liu, H. Zhong, H. Xu, Z. Xu, H. Shao, F. Ding, *ACS Appl. Mater. Interfaces* **2017**, *9*, 13694–13702.
[73] M.-S. Park, Y.-C. Jung, D.-W. Kim, *Solid State Ionics* **2018**, *315*, 65–70.

Manuscript received: July 12, 2024
Revised manuscript received: July 26, 2024
Version of record online: October 17, 2024